Inorg. Chem. **2008**, *47*, 11839−11846

Observation of Staging during Intercalation in Layered α-Cobalt Hydroxides: A Synthetic and Kinetic Study

Yi Du and Dermot O'Hare*

Chemistry Research Laboratory, Department of Chemistry, University of Oxford, Mansfield Road, Oxford, United Kingdom OX1 3TA

Received August 27, 2008

The anion-exchange reaction of the layered α-cobalt hydroxides $Co(OH)_{1.75}(DDS)_{0.25}\cdot 0.6H_2O$ (**1**) and $Co(OH)_{1.7}Cl_{0.3}\cdot 0.4H_2O$ (**3**) with carbonate has been investigated. For **3** the reaction proceeds by complete displacement of the interlayer Cl^- anions by CO_3^{2-} to give $Co(OH)_{1.7}(CO_3)_{0.15}\cdot 0.6H_2O$ (**4**). Remarkably for **1** we only observe ion-exchange of the DDS^- from every other layer to give the second stage intercalate $Co(OH)_{1.75}(DDS)_{0.07}(CO_3)_{0.09}\cdot 0.5H_2O$ (**2**). The kinetics of these processes have been investigated using time-resolved in situ energy dispersive XRD and small/wide-angle X-ray scattering. In both cases the reaction order (*n)* was found to be consistent with a two-dimensional diffusion controlled model. Both **3** and **4** are magnetically ordered, and dc and ac magnetic susceptibility measurements have been used to explore their 3D ferrimagnetically ordered ground states.

Introduction

The development of novel syntheses of heterostructured hybrid materials which combine both organic and inorganic components offers the possibility of preparing new tunable multifunctional materials.[1,2] In this context, the preparation of hybrid nanostructures based on hydrotalcite-like layered hydroxides (LHs) has attracted much interest.[1,3−10]

Recently several groups have reported the synthesis of ordered hybrid LHs nanostructures by the isolation of second stage intercalation compounds.[3,4,9−13] Staging during the intercalation of guest in a layered material describes a phenomenon in which the interlayer galleries fill in a regular periodicity.[1,14] For example, combining the hydrophobic and hydrophilic properties of organic and inorganic LDH intercalates in a single heterostructured phase will produce amphiphilic materials,[14] which may have novel ion-exchange properties.[5,7,9,15,16] For multiatom thick rigid layered hosts such as metal oxides and hydroxides the observation of staging is very rare, and so it is both noteworthy and informative to discover new examples of staging for other layered materials.

Layered cobalt hydroxides are of major interest to both chemists and physicists due primarily to the rich intercalation chemistry combined with the unusual 3D magnetic ordering exhibited by these materials.[17−21] The complex and highly

* To whom correspondence should be addressed. E-mail: dermot.ohare@chem.ox.ac.uk. Fax: +44 1865 285131. Tel: +44 1865 285130.

(1) Taviot-Gueho, C.; Feng, Y. J.; Williams, G. R.; Leroux, F.; O'Hare, D. *Chem. Mater.* **2006**, *18* (18), 4312.
(2) Demessence, A.; Rogez, G.; Rabu, P. *Chem. Mater.* **2006**, *18* (13), 3005.
(3) Iyi, N.; Fujii, K.; Okamoto, K.; Sasaki, T. *Appl. Clay Sci.* **2007**, *35* (3−4), 218.
(4) Zhang, W.; He, J.; Guo, C. *Appl. Clay Sci.* **2008**, *39* (3−4), 166.
(5) Williams, G. R.; O'Hare, D. *J. Phys. Chem. B* **2006**, *110* (22), 10619.
(6) Liu, Z.; Ma, R.; Osada, M.; Iyi, N.; Ebina, Y.; Takada, K.; Sasaki, T. *J. Am. Chem. Soc.* **2008**, *128* (14), 4872.
(7) Duan, X.; Evans, D. G. In *Layered double Hydroxides. Structure & Bonding*; Mingos, D. M. P., Ed.; Springer: Berlin, 2005; Vol. *119*.
(8) Carpani, I.; Berrettoni, M.; Giorgetti, M.; Tonelli, D. *J. Phys. Chem. B* **2006**, *110* (14), 7265.
(9) Williams, G. R.; O'Hare, D. *Chem. Mater.* **2005**, *17* (10), 2632–2640.
(10) Iyi, N.; Kurashima, K.; Fujita, T. *Chem. Mater.* **2002**, *14* (2), 583.
(11) Williams, G. R.; Norquist, A. J.; O'Hare, D. *Chem. Mater.* **2004**, *16* (6), 975.
(12) Fogg, A. M.; Dunn, J. S.; O'Hare, D. *Chem. Mater.* **1998**, *10* (1), 356.
(13) Taviot-Guéhoa, C.; Leroux, F.; Payenb, C.; Bessea, J. P. *Appl. Clay Sci.* **2005**, *28* (1−4), 111.
(14) Ijdo, W. L.; Pinnavaia, T. J. *Chem. Mater.* **1999**, *11* (11), 3227.
(15) Williams, G. R.; O'Hare, D. *J. Mater. Chem.* **2006**, *16* (30), 3065.
(16) Williams, G. R.; Norquist, A. J.; O'Hare, D. *Chem. Commun.* **2003**, (15), 1816.
(17) Ma, R.; Liu, Z.; Takada, K.; Fukuda, K.; Ebina, Y.; Bando, Y.; Sasaki, T. *Inorg. Chem.* **2006**, *45* (10), 3964.
(18) Liu, Z.; Ma, R.; Osada, M.; Takada, K.; Sasaki, T. *J. Am. Chem. Soc.* **2005**, *127* (40), 13869.
(19) Kurmoo, M.; Kumagai, H.; Hughes, S. M.; Kepert, C. J. *Inorg. Chem.* **2003**, *42* (21), 6709.
(20) Kamath, P. V.; Therese, A.; Helen, G.; Gopalakrishnan, J. *J. Solid State Chem.* **1997**, *128* (1), 38.

10.1021/ic801639e CCC: $40.75
Published on Web 11/14/2008

Scheme 1. Schematic Representation of the Reaction of **1** with Carbonate

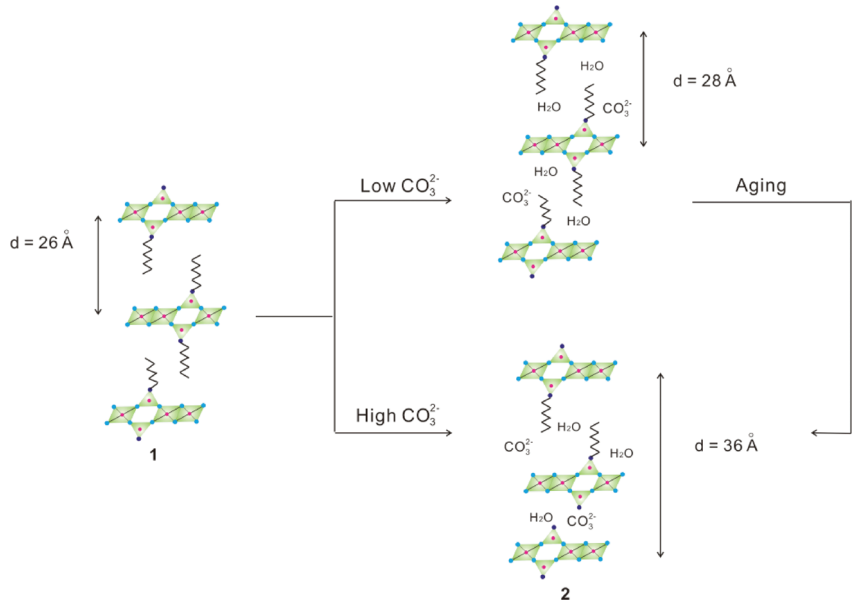

anisotropic magnetic exchange interactions that exist in these materials can be tuned by the introduction of organic or inorganic interlayer anions, and so this offers a possible route to design, or electronic materials.[19,21] However, very few studies describing the intercalation chemistry of cobalt hydroxides have been reported;[18] furthermore, there have been no previous kinetic studies of intercalation in these materials. To date, only first stage intercalation compounds of layered cobalt hydroxides have been reported.[18] Considering the versatility of cobalt hydroxides as functional materials, it is interesting to examine the kinetics of intercalation of anions in cobalt hydroxides and where possible to identify unusual staging intermediates.

In this paper we have investigated the anion-exchange intercalation chemistry of the α-cobalt hydroxides, $Co(OH)_{1.75}(DDS)_{0.25}\cdot 0.6H_2O$ (**1**) and $Co(OH)_{1.7}Cl_{0.3}\cdot 0.4H_2O$ (**3**) with carbonate. To the best of our knowledge, it is the first kinetic study of intercalation in α-cobalt hydroxides. Both first and second staged products of α-cobalt hydroxides have been characterized by elemental analysis (EA), FT-IR, TGA, HRTEM, and SQUID magnetometry. The kinetics and mechanism of the process have been investigated by means of time-resolved, in situ energy dispersive X-ray diffraction (EDXRD) experiments and small-angle X-ray scattering.[5,15,22]

Experimental Section

Synthesis of $Co(OH)_{1.75}(DDS)_{0.25}\cdot 0.6H_2O$ (1) and $Co(OH)_{1.7}Cl_{0.3}\cdot 0.4H_2O$ (3). Green α-cobalt hydroxides, $Co(OH)_{1.75}(DDS)_{0.25}\cdot 0.6H_2O$ (**1**) and $Co(OH)_{1.7}Cl_{0.3}\cdot 0.4H_2O$ (**3**) were prepared via homogeneous precipitation using hexamethylenetetramine (HMT) as the hydrolysis agent.[17,18,23] Typically, the synthesis was performed from a dilute aqueous solution of $CoCl_2\cdot 6H_2O$ (0.6 g), $Na_2C_{12}H_{25}O_4S$ (sodium dodecyl sulfate; NaDDS) (2.0 g)/NaCl (1.0 g), and HMT (2.0 g) under an ambient atmosphere as described by the Sasaki group.[17,18]

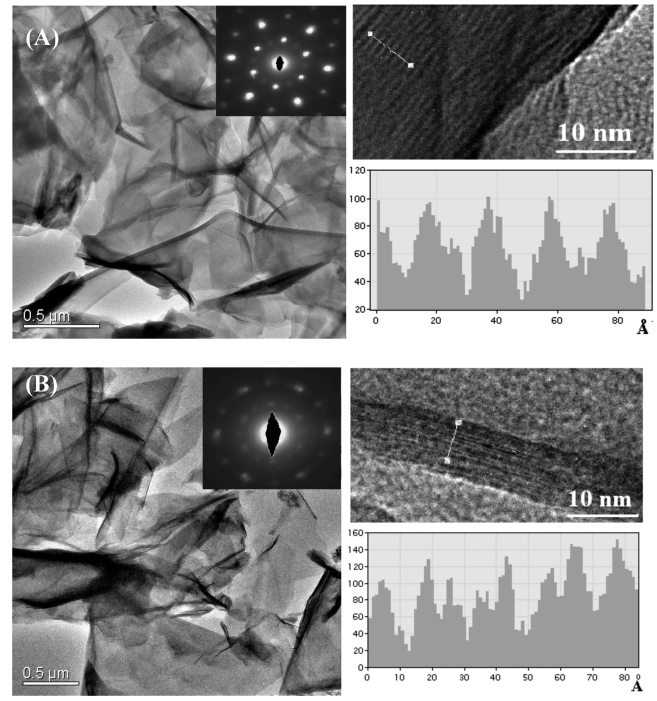

Figure 1. TEM (left), HRTEM (top right), and SAED (left inset) images of (A) **1** and (B) **2**. Inset in (A, B) (bottom right) shows lattice fringes and the corresponding scale bar.

Synthesis of $Co(OH)_{1.75}(DDS)_{0.07}(CO_3)_{0.09}\cdot 0.5H_2O$; (2). A total of 150 mg of **1** was suspended in 4 mL of 0.4 M sodium carbonate solution and heated to between 60 and 120 °C.

Synthesis of $Co(OH)_{1.7}(CO_3)_{0.15}\cdot 0.6H_2O$ (4). A total of 150 mg of **3** was suspended in 4 mL of 2 M sodium carbonate solution and heated to between 80 and 120 °C.

Time-Resolved in Situ Energy-Dispersive X-ray Diffraction (EDXRD) Experiments. Experiments were carried out on Station 16.4 of the U.K. Synchrotron Radiation Source at the Daresbury Laboratory using an experimental setup reported else-

(21) Rabu, P.; Angelov, S.; Legoll, P.; Belaiche, M.; Drillon, M. *Inorg. Chem.* **1993**, *32*, 2463.
(22) Khan, A. I.; O'Hare, D. *J. Mater. Chem.* **2002**, *12* (11), 3191.
(23) Du, Y.; O'Hare, D. *J. Phys. Chem. Solids* **2008**, *69* (5−6), 1040.

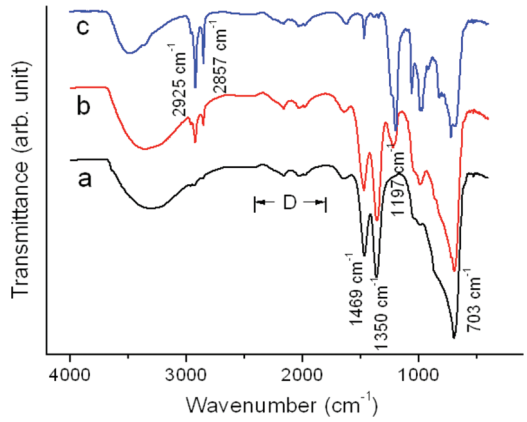

Figure 2. FT-IR patterns for (a) **1**; (b) **2**; and (c) **4**. *Absorptions around 2050 cm^{-1} should be assigned to the substrate absorptions from diamond ATR.

where.[15,22] Aqueous solutions of the guests (saturated CO_3^{2-}) were injected into an ampule **1** or **3**. Individual spectra were collected with acquisition times of 20 s and a fixed detector angle ($2\theta = 1.58°$). Depending on the chosen angle for the three-angle energy discriminating detector a large range of *d*-spacings can be observed between 10 and 60 keV ($d = 50$ to 1.2 Å).

Time-Resolved Small-Angle and Wide-Angle X-ray Scattering (SAXS/WAXS) Experiments. SAXS/WAXS measurements were carried out on beamline 6.2m of the Synchrotron Radiation Source (SRS) at Daresbury Laboratory, Warrington, U.K.[24−26] The beam energy was set at 18.0 keV, corresponding to a wavelength of 0.69 Å. The scattered intensity was recorded using a 200 mm radius quadrant detector located 1.25 m from the sample. The accessible *q* range was thus from 0.013 to 0.45 $Å^{-1}$ ($d = 2\pi/q$). The detector response was calibrated using the scattering from water. The angular scales were calibrated using the scattering peaks of silver behenate ($AgC_{22}H_{43}O_2$) for SAXS and silica for WAXS.

Material Characterization. Fourier transform infrared spectroscopy (FT-IR) spectra of the samples were recorded over a Bio-Rad FTS 6000 spectrometer, spectra recorded within the range of 400−4000 cm^{-1} with 50 scans at 4 cm^{-1} resolution. Elemental analysis (EA) was performed by the analytical services department of the Inorganic Chemistry Laboratory, Oxford University. Thermogravimetric analyses (TGA) were carried out on a Rheometric STA-1500H machine. The sample (ca. 50 mg) was mounted in a corundum crucible and heated at a rate of 5 °C min^{-1} between 25 and 800 °C under a flow of argon. HRTEM was performed on a 4000EX at 400 kV. JEOL Samples were dispersed in ethanol and loaded onto copper grids supporting Formvar film. Magnetic measurements were made using a Quantum Design MPMS-5 SQUID magnetometer. The susceptibility was determined in an applied field of 1 kG after cooling of the sample in both zero applied field (ZFC) and the measuring field (FC). The saturated moment and hysteresis loop were measured at 2 K for ZFC in fields up to 50 kG. AC measurement was performed under 3.5 Oe oscillating field with a frequency of 500 Hz from 2 to 50 K.

Results

Intercalation of CO_3^{2-} in $Co(OH)_{1.75}(DDS)_{0.25}\cdot 0.6H_2O$ (1). Addition of an excess of Na_2CO_3 to the α-cobalt hydroxide $Co(OH)_{1.75}(DDS)_{0.25}\cdot 0.6H_2O$ (**1**) in water at 100 °C leads to the isolation of a phase pure carbonate ion-exchanged product. However, rather than forming the expected first stage carbonate intercalation compound in which all the DDS^- anions had been displaced, a mixed carbonate/DDS product was isolated. All the analytical data indicate that the product contains equal amounts of both DDS^- and CO_3^{2-}, and these ions are ordered to give a stable second stage compound $Co(OH)_{1.75}(DDS)_{0.07}(CO_3)_{0.09}\cdot 0.5H_2O$ (**2**; Scheme 1).

The in situ small angle and wide-angle X-ray scattering (SAXS/WAXS) data for **1** and **2** are shown in Figure S1 (Supporting Information). The Bragg reflections for **1** may be indexed using a rhombohedral unit cell with $a = b = 3.14$ Å, $c = 83.4$ Å. For **2** we observe new Bragg reflections at $d \approx 36.0$ Å, 18.0 Å, and 12.1 Å, respectively. These reflections can be assigned to the 003, 006, and 009 reflections of the second staging layered product **2** (Figure S1b, Supporting Information), which corresponds to the alternate interlayer occupied by DDS^- and CO_3^{2-}. The new cell for **2** is $a = b = 3.06$ Å, $c = 108$ Å. This corresponds to an interlayer repeat distance of 36 Å which is equal to the sum of 27.8 Å (from **1**) and 8.2 Å which is the calculated size required for an intercalated CO_3^{2-} ion. Unfortunately the XRD data on **2** was of poor quality. It appears that on isolation of the sample from the reaction mixture the material becomes highly disordered and poorly crystalline especially along the [001] direction. The XRD data for both **1** and **2** are shown in Figure S2 (Supporting Information). The 003 and 006 Bragg reflections of **1** are very sharp and symmetric. However, a broad feature due to the 003 Bragg reflection was observed for **2**. On the other hand, the relative intensity of the 110 Bragg reflections for both **1** and **2** are very similar.

Both **1** and **2** were studied by high-resolution transmission electron microscopy (HRTEM) and selected area electron diffraction (SAED) with a view to probe the symmetry of the crystalline domains and the interlayer stacking arrangements. Figure 1a,b shows TEM images of **1** and **2**, respectively. Both the corresponding selected area electron diffraction (SAED) patterns (inset in Figure 1) can be indexed as a two-dimensional in-plane hexagonal lattice. This implies that the platelets are lying on their {001} zone axis direction.[27] The HRTEM images for **1** show lattice fringes separated by 2.6 nm. The HRTEM images for **2** show a series of lattice fringes composed of a thinner layer of 0.8 nm thickness and a thicker layer of 2.8 nm, which is consistent with the above-mentioned second staging structure model. Furthermore, this alternating thickness interlayer arrangement extends over long length scales. In agreement with the XRD data, a disordered stacking arrangement was observed when the solvent was removed for **2**. The SAXS, XRD, and HRTEM data all support a second stage anion ordering arrangement

(24) Fan, W.; Ogura, M.; Sankar, G.; Okubo, T. *Chem. Mater.* **2007**, *19* (8), 1906.
(25) Panzarella, B.; Tompsett, G.; Conner, W. C.; Jones, K. *Chem. Phys. Chem.* **2007**, *8* (3), 357.
(26) Cernik, R. J.; Barnes, P.; Bushnell-Wye, G.; Dent, A. J.; Diakun, G. P.; Flaherty, J. V.; Greaves, G. N.; Heeley, E. L.; Helsby, W.; Jacques, S. D. M.; Kay, J.; Rayment, T.; Ryan, A.; Tang, C.; Terrilla, N. J. *J. Synchrotron Rad.* **2004**, *11*, 163.
(27) Du, Y.; O'Hare, D. *Inorg. Chem.* **2008**, *47* (8), 3234.

Table 1. Summary of the Elemental Microanalysis Data for **1**−**4**

compound	elemental composition obsd (calcd), % N	C	H	formula
1	0.06 (−)	21.65 (21.71)	5.64 (5.59)	$Co(OH)_{1.75}(DDS)_{0.25}\cdot 0.6H_2O$
2	0.04 (−)	9.1 (9.17)	3.66 (3.72)	$Co(OH)_{1.75}(C_{12}H_{25}O_4\ S)_{0.07}(CO_3)_{0.09}\cdot 0.5H_2O$
3		0.04 (−)	2.44 (2.36)	$Co(OH)_{1.7}Cl_{0.3}\cdot 0.4H_2O$
4		1.62 (1.65)	2.74 (2.71)	$Co(OH)_{1.7}(CO_3)_{0.15}\cdot 0.6H_2O$

Table 2. Summary of the Kinetic Data Summary for the Conversion of **1** to **2**

T, °C	n^a	k^a, 10^{-3} s^{-1}	k^b, 10^{-3} s^{-1}	$t_{0.5}{}^c$, s
120	1.20 ± 0.04	4.59 ± 0.08	4.57 ± 0.09	165
100	1.00 ± 0.03	2.95 ± 0.06	2.96 ± 0.05	223
80	1.06 ± 0.02	1.95 ± 0.03	1.97 ± 0.03	371
60	1.14 ± 0.05	1.30 ± 0.04	1.30 ± 0.04	555

[a] Least squares fit to the Avrami-Erofe'ev model: $\alpha = 1 - \exp\{-[k(t - t_{ind})]^n\}$. [b] Least squares fit to model: $\alpha = 1 - \exp\{-[k(t - t_{ind})]^1\}$. [c] $t_{0.5}$ is defined as the time when $\alpha(t)/\alpha(t = \infty) = 0.5$.

Table 3. Summary of the Kinetic Data Summary for the Conversion of **3** to **4**

T, °C	n^a	k^a, 10^{-3} s^{-1}	k^b, 10^{-3} s^{-1}	$t_{0.5}{}^c$, s
120	1.18± 0.05	3.92 ± 0.08	3.88 ±0.11	192
110	1.34 ± 0.03	2.26 ± 0.03	2.19 ± 0.08	332
100	1.22 ± 0.07	1.98 ±0.06	2.02 ± 0.08	363
90	1.00 ± 0.07	1.44 ± 0.06	1.44 ± 0.06	503
80	1.20 ± 0.06	1.12 ± 0.02	1.13 ± 0.03	725

[a] Least squares fit to the Avrami-Erofe'ev model: $\alpha = 1 - \exp\{-[k(t - t_{ind})]^n\}$. [b] Least squares fit to model: $\alpha = 1 - \exp\{-[k(t - t_{ind})]^1\}$. [c] $t_{0.5}$ is defined as the time when $\alpha(t)/\alpha(t = \infty) = 0.5$.

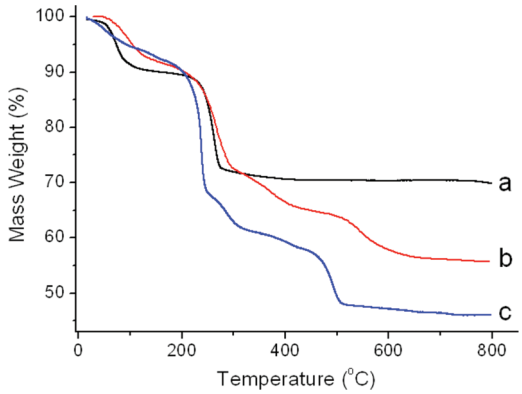

Figure 3. TGA traces for (a) **1**; (b) **2**; and (c) **4**.

for **2**. The coexistence of both DDS^- and CO_3^{2-} was further confirmed by FT-IR and TGA experiments.

Vibrational spectroscopy has proved to be the principal method for studying the existence and bonding mode of CO_3^{2-} and DDS^- in metal complexes. The IR spectrum of **2** is shown in Figure 2 with **4** as the reference. A broad absorption ca. 3400 cm^{-1} can be assigned to the O−H stretching modes of interlayer water molecules while the other broad absorption at low-frequency region (~700 cm^{-1}) is ascribed to Co−O stretching and Co−OH bending vibrations in the brucite-like octahedral sheet.[18] The two bands at 1350 and 1469 cm^{-1} are characteristic of the presence of carbonate ions indicating a low site symmetry (C_{2v}) for the CO_3^{2-} ions.[18,28] The absorption bands at around 2857−2925 cm^{-1} and 1197 cm^{-1} displayed in Figure 2a,b are characteristic of the aliphatic and sulfate groups of DDS anions, respectively.[18,29]

Thermogravimetric analysis (TGA) was performed to investigate the chemical composition and to gain insight into the thermal decomposition processes. All these results are consistent with the formula we proposed for **2** and the elemental microanalysis data (Table 1). TGA data of **1** and **2** were shown in Figure 3 with **4** as reference. Both **1** and **2** exhibit a three-step weight loss separated in the range <100 °C, 150−250 °C, and 300−500 °C. The first weight loss (~7% in both cases) is classically attributed to the evolution of absorbed and intercalated water.[28] The subsequent weigh losses are consistent with the substitution of significant amounts of DDS^- by CO_3^{2-}. In the case of both **1** and **2**, the product remained after heating to 800 °C is confirmed to be crystalline CoO and amorphous carbon by XRD and EA.

Time-resolved, in situ EDXRD data was collected following the addition of **1** to 4 mL of 0.4 M Na_2CO_3 at 120 °C. A three-dimensional stack plot of the in situ EDXRD data is shown in Figure 4. The data clearly indicates the one-step nature of the formation of second stage product **2**. The extent of reaction (α), where $\alpha(t) = I_{hkl}(t)/I_{hkl}(\max)$, vs time curve was observed to cross close to $\alpha = 0.4$ indicating that no intermediates are involved, and the contour plot clearly shows the growth of a Bragg reflection at higher d-spacing (36 Å, 19.5 keV) which is assigned as the 003 Bragg reflection in **2**.

Time-resolved, in situ EDXRD data was collected at lower concentrations of Na_2CO_3 (0.2 M) reveals the existence of a crystalline intermediate phase with a slightly enhanced interlayer repeat. The best explanation we have for this observation is the transient formation of a hydration form of the sulfate group within the layers which expands the interlayer distance and/or partial diffusion of CO_3^{2-} anions into the interlayer region as indicated in Scheme 1.[29] If the reaction was performed at even lower carbonate concentrations, then the reaction did not go to completion, while at higher concentrations it became too fast to monitor. Using an intermediate concentration, we were able to carry out a kinetic analysis of the reaction.

The temperature dependence of this reaction was investigated over the range 60−120 °C. In each case, the Avrami-Erofe'ev model, $[-\ln(1 - \alpha)]^{1/n} = k(t - t_{ind})$, where $\alpha(t) = I_{hkl}(t)/I_{hkl}(\max)$,[5,9,11,15] was fitted to the experimental data (Figure 5) to calculate the value of the reaction exponent n and the rate constant k. A linear Sharp-Hancock plot $\{\ln(-\ln(1 - \alpha))$ vs $\ln(t)\}$[7,12,22] indicates that the Avrami-Erofe'ev formalism could be used to quantify the kinetic data as shown in Figure S3 (Supporting Information). The kinetic data are summarized in Table 2. As is intuitively anticipated,

(28) Tessier, C.; Guerlou-Demourgues, L.; Faure, C.; Demourgues, A.; Delmas, C. *J. Mater. Chem.* **2000**, *10* (5), 1185.

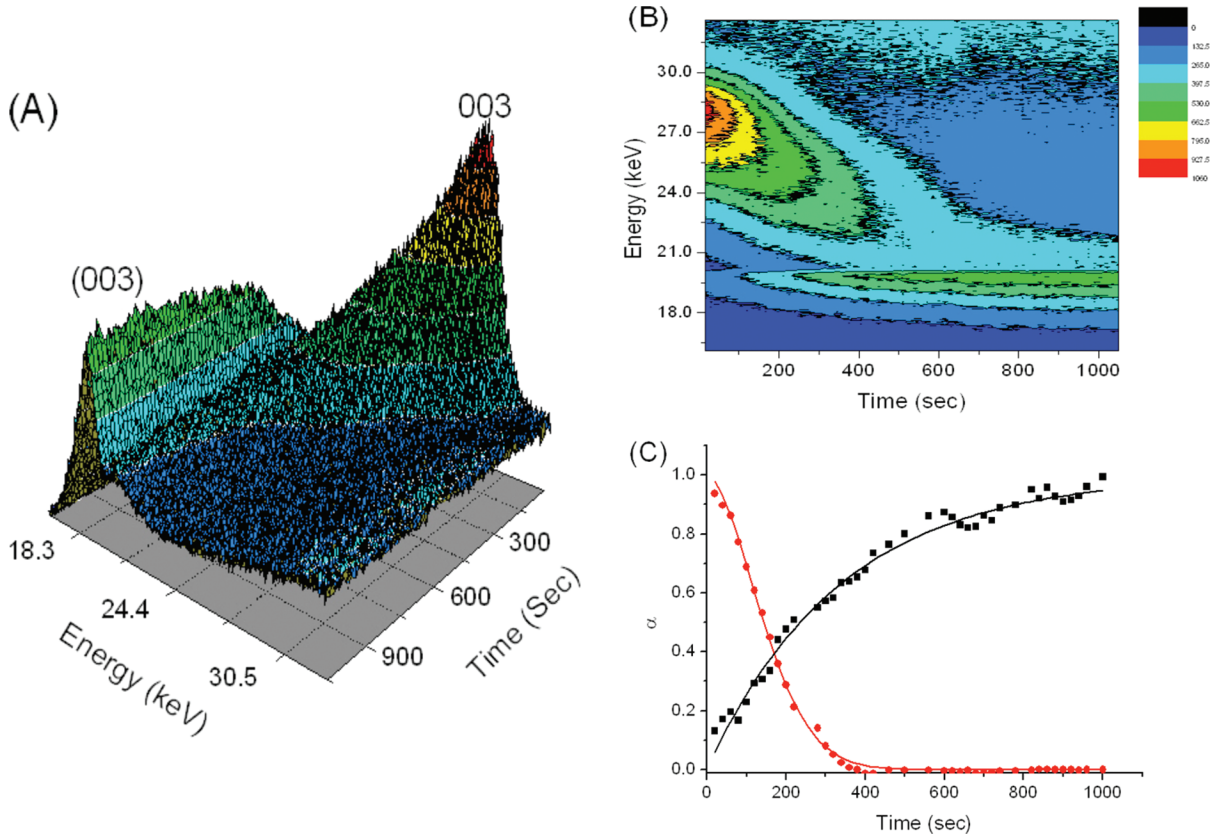

Figure 4. In situ EDXRD data during the course of the reaction between 120 mg of **1** and 4 mL of 0.5 M Na_2CO_3 at 120 °C: (a) 3D stack plot showing the evolution of the 003 Bragg reflection for **1** and the 003 Bragg reflection for **2**; (b) contour plot; (c) the corresponding plot of extent of reaction (α) vs time (*t*).

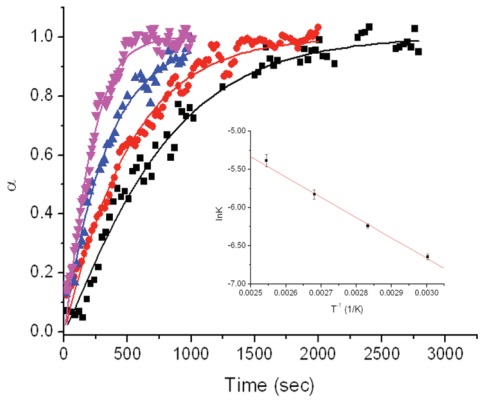

Figure 5. Temperature dependence of extension of reaction (α) plotted against time (*t*). The data have been fitted with Avrami-Erofe'ev equation at 60 °C (pink triangles), 80 °C (blue triangles), 100 °C (red circles), and 120 °C (black squares), respectively. Inset: Arrhenius plot for the phase conversion from **1** to **2**.

the reaction rate increased with temperature and no induction time is observed in all cases.

The Avrami exponent (*n*) was found to be close to 1 over all the temperature studied. *n* is then fixed to be 1, and the subsequent rate constant *k* was found to be consistent as shown in Table 2. Plots of α vs reduced time ($t/t_{0.5}$) were found to be superimposable, confirming that the same mechanism is operational in each case.[7,9] The value of the exponent (*n*) is consistent with a two-dimensional diffusion controlled kinetic model, which means the rate-limiting step is likely to be the diffusion of CO_3^{2-} anions into the crystal. At lower temperatures, a greater amount of scatter in the data is observed because of the lower crystallinity of product with respect to the ones generated at elevated temperatures.[7,12,22] The activation energy is calculated to be ~22.77(6) kJ mol^{-1} from a plot of ln *k* vs 1/*T* as inset in Figure 5 on the basis of Arrhenius equation, $k = Ae^{-E_a/RT}$.

Intercalation of CO_3^{2-} in $Co(OH)_{1.7}Cl_{0.3}\cdot 0.4H_2O$ (3). Addition of an excess of Na_2CO_3 to the layered α-cobalt hydroxide $Co(OH)_{1.7}Cl_{0.3}\cdot 0.4H_2O$ (**3**) leads to the facile exchange of Cl^- for CO_3^{2-} and the formation to a stable first stage compound $Co(OH)_{1.7}(CO_3)_{0.15}\cdot 0.6H_2O$ (**4**).

The XRD data for **3** and **4** are shown in Figure S4 (Supporting Information). The Bragg reflections for **3** may be indexed using the rhombohedral unit cell with $a = b =$ 3.14 Å, $c = 24.0$ Å. A full characterization on **3** has been made by the Sasaki group.[12,13] For **4** we observe new Bragg reflections at $d \approx 8.7$ Å and 4.3 Å. These reflections can be assigned to the 003 and 006 reflections from a new unit cell with $a = b = 3.12$ Å, $c = 26.1$ Å. The interlayer repeat distance is 8.7 Å which is the calculated size required for an intercalate CO_3^{2-} ion. FT-IR and TGA data for **4** are shown in Figures 2 and 3 with elemental analysis data in Table 1.

Time-resolved, in situ EDXRD data was collected following the addition of **3** to 4 mL of 2 M Na_2CO_3 at100 °C. The EDXRD shows that **3** transforms directly to the first staging compound **4** without the observation of any intermediate phases (Figure 6). The temperature dependence of this reaction was investigated over the range 80−120 °C with

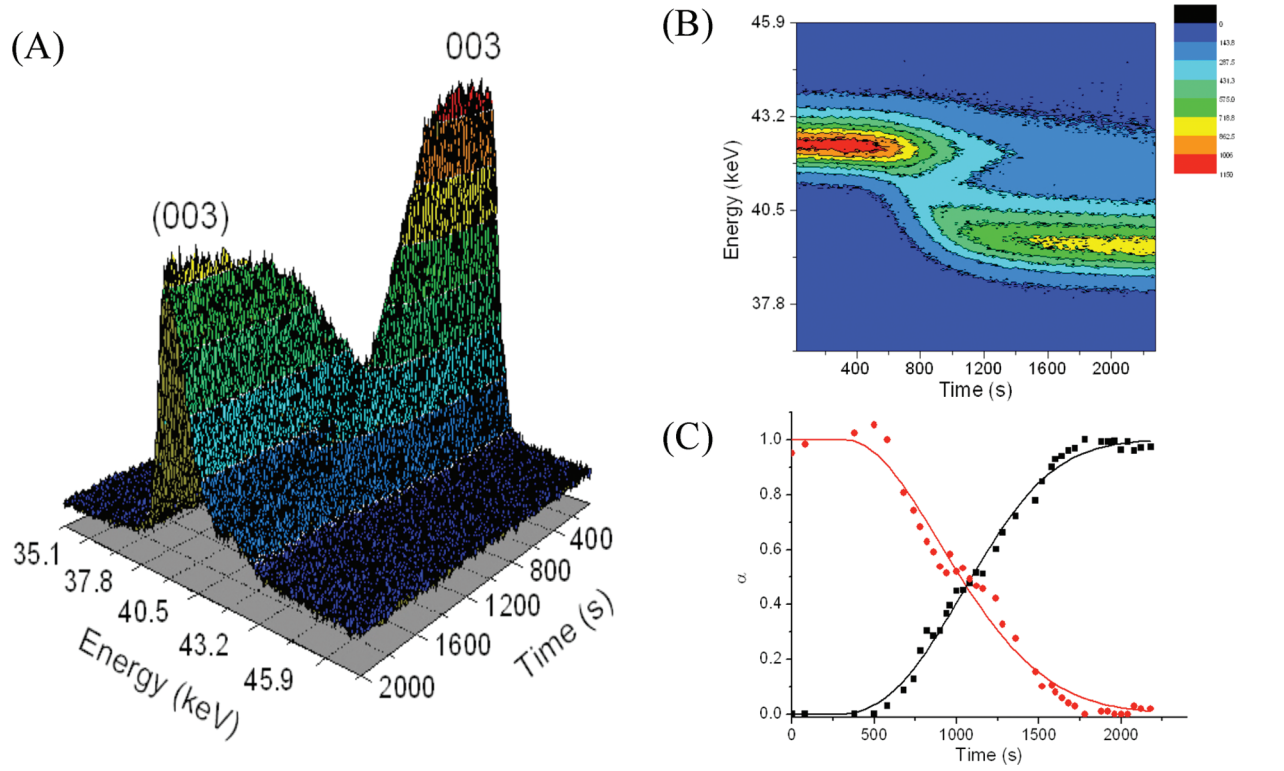

Figure 6. In situ EDXRD data during the course of the reaction between 120 mg of **3** and 4 mL 0.5 M Na_2CO_3 at 100 °C: (a) 3D stack plot showing the evolution of the 003 Bragg reflections for **3** and the 003 Bragg reflections of **4**; (b) contour plot; (c) the corresponding plot of extent of reaction (α) vs time (*t*).

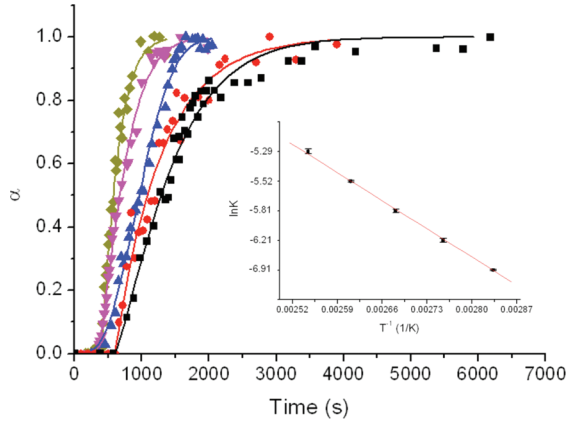

Figure 7. Temperature dependence of extension of reaction (α) vs time (*t*). The data have been fitted with Avrami-Erofe'ev equation at 120 °C (dark yellow diamonds), 110 °C (pink triangles), 100 °C (blue triangles), 90 °C (red circles), and 80 °C (black squares), respectively. Inset: Arrhenius plot for the phase conversion from **3** to **4**.

4 mL of 2 M Na_2CO_3. At each temperature, the Avrami-Erofe'ev model was fitted to the experimental data (Figure 7) to calculate the value of the reaction exponent *n* and the rate constant *k*. The data give a linear Sharp-Hancock plot. The kinetic data are summarized in Table 3. Plots of α vs reduced time ($t/t_{0.5}$) were found to be superimposable, confirming that the same mechanism is operational in each case.[7,9] The value of the exponent (*n*) is consistent with a two-dimensional diffusion controlled model following a much higher activation energy ~112.8(11) kJ mol^{-1} calculated from Arrhenius equation (inset in Figure 7). It is consistent with the fact that the diffusion of CO_3^{2-} into **3** is more difficult compared to **1** because **3** needs extra energy to expand the interlayer in order to accommodate the bigger anion CO_3^{2-}. In addition, the intercalated anions become covalent bonded to the cobalt centers so the magnitude of the activation energy of this type of α-cobalt hydroxide based anion exchange reaction is bigger than the common anion exchange reaction for layered double hydroxides.[7,11,12,16]

Figure 8 shows the temperature-dependent dc molar magnetic susceptibility of **1**, **2**, and **4** (Figure 8c) in an applied field of 1000 Oe after zero-field-cooling (ZFC) and field-cooling (FC) measurements. A very clear and sharp bifurcation point is evident in all three samples, at 8.2, 6.3, and 16.5 K, respectively. The plot of χ_{mol}^{-1} vs *T* shows that all three materials obey the Curie−Weiss law above ca. 125 K giving effective magnetic moment (μ_{eff}) of 5.0 μ_B, 5.2 μ_B, and 4.6 μ_B for **1**, **2**, and **4**, respectively. These are all slightly higher than the spin-only value for $S = 3/2$ ions but are within the range of high-spin mixed octahedral/tetrahedral cobalt(II) compounds.[19,21]

The isothermal magnetization *M*(*H*) at 2 K for **1**, **2**, and **4** (Figure 9) shows hysteresis loops consistent with a 3D magnetically ordered ground state, which is further confirmed by ac susceptibility measurement as shown in Figure 10. The saturation magnetizations are 1.28 μ_B, 1.37 μ_B, and 1.16 μ_B, for **1**, **2**, and **4**, respectively, which could be explained by a model based on two antiferromagnetically coupled sublattices. For **2** this could be formulated as $[Co^{(oct)}_{0.75}Co^{(tet)}_{0.25}(OH)_{1.75}]^{0.25+}(CO_3)_{0.09}(DDS)_{0.07}\cdot 0.6H_2O$. Therefore, the saturation magnetization can be calculated as $(g_{oct} \times Co^{(oct)} - g_{tet} \times Co^{(tet)}) \times S = (2 \times 0.75 - 2 \times 0.25) \times 1.5 = 1.5\ \mu_B$, which is consistent with the experimental value 1.37 μ_B. Calculations using a similar

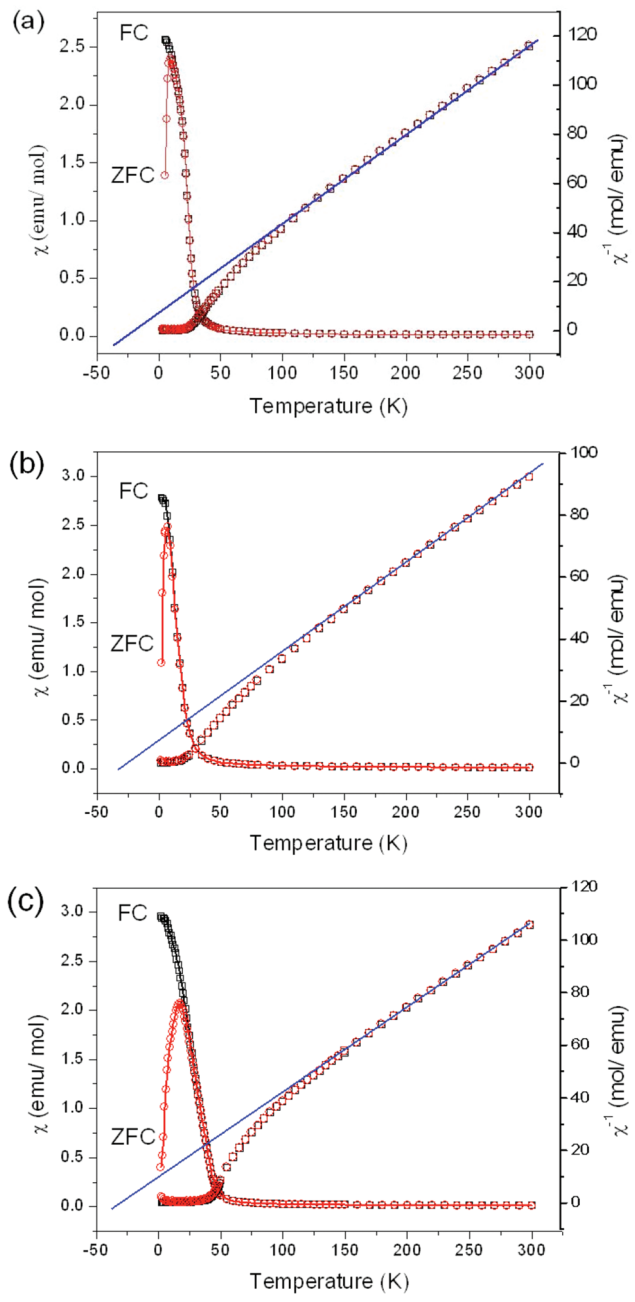

Figure 8. (a) Plot of χ_M and χ_M^{-1} vs T for **4**; data following cooling in 1 kG field (□; FC) and zero applied field (○; ZFC). (b) Plot of χ_M and χ_M^{-1} vs T for **2**; data following cooling in 1 kG field (□; FC) and zero applied field (○; ZFC). (c) Plot of χ_M and χ_M^{-1} vs T for **1**; data following cooling in 1 kG field (□; FC) and zero applied field (○; ZFC).

magnetic model for **1** and **4** give predicted saturation moments of 1.5 μ_B and 1.2 μ_B, which is in good agreement with the experimental values 1.28 μ_B and 1.16 μ_B. The existence of the long-range magnetic order has been described by several other groups to explain the magnetic properties of related layered cobalt hydroxides.[17,21,30−34]

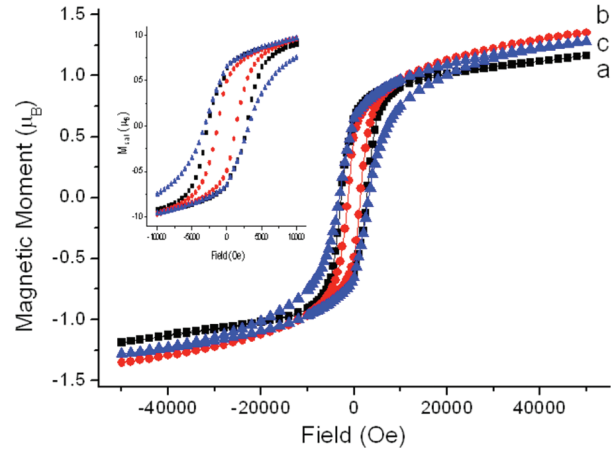

Figure 9. Field dependence of the molar magnetization for (a) **4**; (b) **2**; and (c) **1** at 2 K from −5 to 5 T.

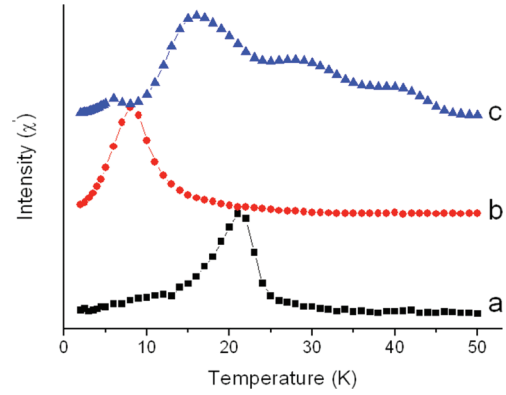

Figure 10. Real component of the magnetic susceptibility (χ') as a function of temperature for (a) **4**; (b) **2**; and (c) **1** under 3.5 Oe ac field and at a frequency of 500 Hz.

The temperature dependence of ac magnetic susceptibility for **1**, **2**, and **4** was measured in the temperature range 2−50 K under an oscillating magnetic field of 3.5 Oe (under a near zero dc field of 5 Oe) (Figure 10). Spontaneous magnetic ordering for 3D magnets is characterized by a discontinuous jump in dc magnetization which coincides with the peak in the in-phase ac magnetization (Figure 10) and to the nonzero out of phase (not shown) ac magnetization. The peaks in both real (in phase) and imaginary (out of phase) components of the ac susceptibilities are taken to be indicative of a ferrimagnetic 3D ordering transition. The Curie temperature, T_C, of the samples, was determined to be 31, 9, and 22 K (center peak) for **1**, **2**, and **4**, respectively. The broad peak for **1** could be attributed to its highly crystalline nature. The low value of T_C for **2** must be largely due to the much poorer crystallinity.

Conclusions

The second stage intercalation compound $Co(OH)_{1.75}(DDS)_{0.07}(CO_3)_{0.09}\cdot 0.5H_2O$ (**2**) has been characterized. In order to form this material half of the DDS^- anions in $Co(OH)_{1.75}(DDS)_{0.25}\cdot 0.6H_2O$ (**1**) has resisted ion-exchange

(29) Bubniak, G. A.; Schreiner, W. H.; Mattoso, N.; Wypych, F. *Langmuir* **2002**, *18* (16), 5967.
(30) Ben Salah, M.; Vilminot, S.; Andre, G.; Richard-Plouet, M.; Mhiri, T.; Takagi, S.; Kurmoo, M. *J. Am. Chem. Soc.* **2006**, *128* (24), 7972.
(31) Ben Salah, M.; Vilminot, S.; Andre, G.; Bouree-Vigneron, F.; Richard-Plouet, M.; Mhiri, T.; Kurmoo, M. *Chem. Mater.* **2005**, *17* (10), 2612.
(32) Mohsen, B. S.; Vilminot, S.; Richard-Plouet, M.; Andre, G.; Mhiri, T.; Kurmoo, M. *Chem. Commun.* **2004**, (22), 2548.
(33) Forster, P. M.; Tafoya, M. M.; Cheetham, A. K. *J. Phy. Chem. Solids* **2004**, *65* (1), 11.
(34) Kurmoo, M. *J. Mater. Chem.* **1999**, *9*, 2595.

by an excess of carbonate. We have found only one other example of second stage intermediates involving carbonate anions.[4] The activation energy for the intercalation of **1** with carbonate is much lower than that for **3** which may be a factor in the observation of staging. However, it is still not clear why treatment of **1** with carbonate gives only a second stage product, while the same reaction with **3** gives a first stage product. The temperature dependence of the kinetics suggest that the reactions follow a two-dimensional diffusion controlled model. Magnetic measurements show that all the materials behave as 3D ferrimagnets at low temperature.

Acknowledgment. The authors thank Clarendon Scholarship and Balliol College, Oxford University, for funding, and the CCLRC for access to the UK SRS. Also, thanks to Dr. Dave Taylor and Dr. Tony Bell at Station 16.4 and Dr. Chris Marin at Station 6.2m, on the SRS Daresbury Laboratory, UK, for experimental set up and data processing.

Supporting Information Available: In situ SAXS and WAXs, XRD, Sharp-Hancock plot, and FESEM. This material is available free of charge via the Internet at http://pubs.acs.org.

IC801639E